EPJ Web of Conferences **121**, 03006 (2016) DOI: 10.1051/epjconf/201612103006
RICAP-2014

Positron fraction, electron and positron spectra measured by AMS-02

Cecilia Pizzolotto[1,2,a] for the AMS-02 Collaboration

[1] INFN, Sezione di Perugia, 06123 Perugia, Italy
[2] INFN, Sezione di Tor Vergata, 00133 Roma, Italy

Abstract. A precise measurement by AMS-02 of the electron spectrum up to 700 GeV and of the positron spectrum and positron fraction in primary cosmic rays up 500 GeV are presented. The combined measurement of the cosmic-ray electron and positron energy spectra and fraction provide a unique tool to improve our understanding of the production, acceleration and propagation mechanism of cosmic rays.

1. Introduction

The first results from AMS-02 on the positron fraction generated widespread interest and discussions on the origin of high-energy positrons [1]. Here we present the new results on the positron fraction and the individual electron and positron fluxes measurements in an extended energy range, all together these measurements will provide insight into the origin of cosmic rays.

2. AMS-02 detector

The AMS-02 detector [2] consists of a permanent magnet, nine planes of precision silicon tracker, a transition radiation detector (TRD), four planes of time-of-flight (TOF) counters, an array of anticoincidence counters, a ring imaging Cherenkov detector, and an electromagnetic calorimeter (ECAL). AMS-02 operates continuously on the ISS and is monitored and controlled around the clock from the ground. The timing, location, and attitude are determined by a combination of GPS units affixed to AMS-02 and to the ISS.

The TRD (above the magnet), the ECAL (below the magnet) and the tracker provide clean and redundant identification of positrons and electrons with independent suppression of the proton background. The matching of the ECAL energy, E, and the momentum measured with the tracker, p, greatly improves the proton rejection.

3. Data sample and event selection

In the positron fraction analysis, to differentiate between $e^{\pm}$ and protons in the TRD, signals from the 20 layers of proportional tubes are combined in a TRD estimator formed from the ratio of the log-likelihood probability of the $e^{\pm}$ hypothesis to that of the proton hypothesis in each layer. A similar approach is used in the individual flux measurements, where only the

[a] e-mail: cecilia.pizzolotto@pg.infn.it

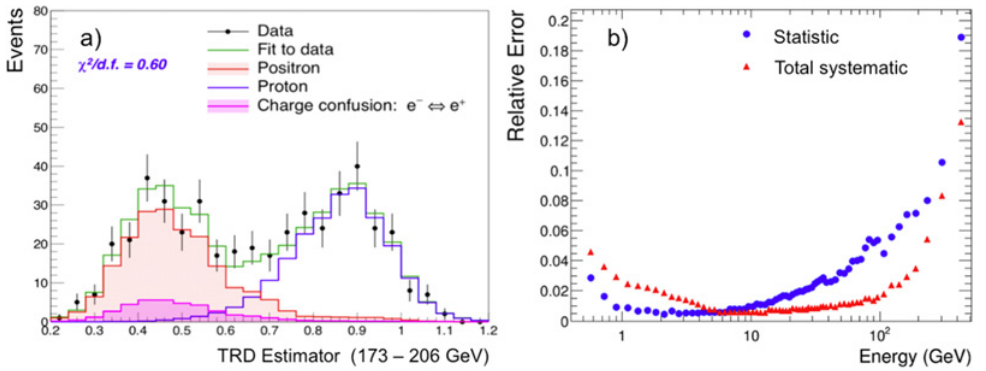

Figure 1. Panel a) shows the results of a 2D fit on the TRD estimator for the positive sample: data points (black) are fitted with the sum of proton (blue), positron (red) and charged confused electrons (magenta) contributions. Panel b) shows the relative statistic and total systematic error as a function of the energy for the positron fraction measurement. The statistical error dominates above 5 GeV.

log-likelihood probability of the $e^{\pm}$ is used as a discriminator. The proton rejection power of the TRD estimator at 90% $e^{\pm}$ efficiency measured on orbit is 10^3 to 10^4 [3].

To cleanly identify electrons and positrons in the ECAL, an estimator, based on a boosted decision tree algorithm [4], is constructed using the 3D shower shape in the ECAL. The proton rejection power of the ECAL estimator reaches 10^4 when combined with the energy-momentum matching requirement $E/p > 0.75$ [3].

Similar selection cuts are applied for the positron fraction and for the separate flux measurements: events are selected by requiring a track in the TRD and in the tracker, a cluster of hits in the ECAL, and a measured velocity $\beta \sim 1$ in the TOF consistent with a downward-going |Z|=1 particle. The tracker measures the sign of the charge. To reject the bulk of the remaining protons, an energy-dependent cut on the ECAL estimator is applied. To reject secondary positrons and electrons produced by the interaction of primary cosmic rays with the atmosphere, the energy measured with the ECAL is required to exceed, by a factor of 1.2, the maximum Størmer cutoff [5] for either a positron or electron at the geomagnetic location where the particle was detected and at any angle within the acceptance.

For the positron fraction a total of 10.9 million positron and electron events are presented. In the separate fluxes a total of 9.23×10^6 events are identified as electrons and 0.58×10^6 as positrons. These numbers are slightly less than the numbers in the positron fraction due to tighter selection criteria, such as on the exposure time, used to minimize the uncertainty of the separate flux measurements.

4. Positron fraction analysis

In each energy bin, the two-dimensional reference spectra for $e^{\pm}$ and the background are fit to data in the [TRD estimator–log(E/p)] plane by varying the normalizations of the signal and the background. The fit is performed simultaneously for the positive and negative rigidity data samples in each energy bin yielding the number of positrons, the number of electrons, the number of protons, and the amount of charge confusion. The charge confusion is defined as the fraction of electrons or positrons reconstructed with a wrong charge sign. Figure 1a shows the results of the fit on the TRD Estimator in the energy range 173–206 GeV.

Different sources of systematic errors have been carefully investigated. Compared to the previous positron fraction publication [3], systematic errors decreased with increasing

statistics in the high energy region. Above 5 GeV the total systematic errors are negligible compared to the statistical ones as illustrated in Fig. 1b.

Above 100 GeV charge confusion is the dominant systematic error. There are two main sources of charge confusion: the first source is related to the finite resolution of the tracker and multiple scattering, the second to the production of secondary tracks along the path of the primary $e^{\pm}$ in the tracker. Both sources of charge confusion are found to be well reproduced by the Monte Carlo simulation and their reference spectra are derived from the Monte Carlo simulation. The systematic uncertainties due to these two effects were examined in each energy bin. To evaluate the systematic uncertainty related to event selection, the complete analysis is repeated in every energy bin over 1000 times with different cut values, such that the selection efficiency varies up to 30%. The reference spectra are determined from high statistics electron and proton data samples selected using tracker and ECAL information including charge sign, track-shower axis matching, and the ECAL estimator. The purity of each reference spectrum is verified using Monte Carlo simulation. The systematic error associated with the uncertainty of the data derived reference spectra arises from their finite statistics. The error is measured by varying the shape of the reference spectra within the statistical uncertainties. These contributions to the systematic uncertainty are mainly negligible. Below 5 GeV, the energy scale is the dominant contribution to the systematic uncertainty of the measurement. The energy scale is verified by using minimum ionizing particles and comparing data to the test beam where the beam energy is known with precision and this results in a negligible contribution to the total systematic error at energies above 5 GeV.

AMS-02 has measured the positron fraction as a function of energy from 0.5 to 500 GeV [3, 6]. Compared to previous measurements, AMS-02 extends the energy range and provides higher precision. Below $\sim$ 8 GeV, the positron fraction decreases rapidly with energy as expected from the diffuse production of positrons [7]. The fraction increases steadily from 10 to $\sim$250 GeV, but from 20 to 250 GeV the slope decreases by an order of magnitude. Above $\sim$200 GeV the positron fraction no longer increases with energy.

5. Positron and electron fluxes analysis

The isotropic fluxes of cosmic-ray electrons (Φ_{e^-}) and positrons (Φ_{e^+}) in the energy bin E of width ΔE are given by

$$\Phi_{e^{\pm}} = \frac{N_{e^{\pm}}(E)}{A_{eff}\epsilon_{trig}T(E)\Delta E} \tag{1}$$

where N_{e^-} is the number of electrons, N_{e^+} is the number of positrons, A_{eff} is the effective acceptance, ϵ_{trig} is the trigger efficiency, and T is the exposure time.

The effective acceptance is defined as $A_{eff} = A_{geom}\epsilon_{sel}\epsilon_{id}(1+\delta)$ where A_{geom} is the geometric acceptance corresponding to $\simeq 550$ cm^{2}sr, ϵ_{sel} is the selection efficiency, ϵ_{id} is the identification efficiency for electrons or positrons, and δ is a minor correction obtained from the comparison of selection efficiencies for data and Monte Carlo. This correction δ is found to be a smooth, slowly falling function of energy, with a value $\sim$2% at 10 GeV and $\sim$6% at 700 GeV. The selection efficiency ϵ_{sel} is determined from the Monte Carlo simulation and found to be a smooth function of energy with a value of $\sim$70% at 100 GeV.

The trigger efficiency ϵ_{trig} is determined from data. It is 100% above 3 GeV decreasing to 75% at 1 GeV.

The exposure time as a function of energy $T(E)$ is determined by counting the live time weighted number of seconds at each location where the geomagnetic cutoff requirement is

satisfied. The exposure time for this analysis at 5 GeV is 1.4×10^7 s, at 10 GeV it is 3.2×10^7 s, and above 30 GeV it is constant at 6.1×10^7 s.

In each energy bin, a two-step fit procedure is performed to determine N_{e^+} and N_{e^-}. First, a template fit is used to find the number of electrons plus positrons reconstructed with a positive charge sign N^+ and the number of electrons plus positrons reconstructed with a negative charge sign N^-. The TRD templates, that is, the shapes of the TRD likelihood distributions for signal and background, are determined from data by selecting clean samples of electrons and protons using the ECAL estimator and the charge sign measured by the tracker. The TRD templates for electrons and positrons are identical. They are found to be independent of energy above 10 GeV. A maximum-likelihood fit of the resulting TRD templates to the data yields N^+, N^-, and the number of protons in the bin. Second, N^+ and N^- are corrected for charge confusion: in each energy bin, two tracker templates are defined, one for particles with correctly reconstructed charge sign and another for particles with wrongly reconstructed charge sign. The former is defined using the negative rigidity data sample. The latter is based on the Monte Carlo simulation. These tracker templates are fit to data, bin by bin, to obtain the amount of charge confusion resulting in the determination of N_{e^+} and N_{e^-}.

An accurate study of the sources of systematic error has been carried on, in a way similar to what already descrided for the positron fraction. The systematic error associated with the uncertainty of the template shapes, of effects of charge confusion, the effective acceptance, energy scale and event selection have been considered. The total systematic error is taken as the quadratic sum of these contributions and the minute bin-to-bin migration systematic. As an example, in the energy bin from 59.1 to 63.0 GeV, the statistical error on the positron flux is 4.9% and the total systematic error is 2.9% with 0.8% from the TRD templates, 0.4% from charge confusion, 2.8% from the effective acceptance, and 0.2% from bin-to-bin migration.

The electron flux has been measured from 0.5 to 700 GeV and the positron flux from 0.5 to 500 GeV extending the measurement to higher energies than previous experiments and with better precision [8]. Below ∼10 GeV, the behavior for both electrons and positrons is affected by solar modulation as seen in our data by variations of the fluxes over this data-taking interval. However, above ∼20 GeV the effects of solar modulation are insignificant within the current experimental accuracy. The data show that above ∼20 GeV and up to 200 GeV the electron flux decreases more rapidly with energy than the positron flux, that is, the electron flux is softer than the positron flux. This is not consistent with only the secondary production of positrons [7]. Neither the electron flux nor the positron flux can be described by single power laws ($\propto E^{\gamma}$) over the entire range.

6. Minimal fit model

We use a minimal model to fit the data of the positron fraction and of the total ($e^+ + e^-$) flux presented in [9]. In this model the e^- and e^+ fluxes are parametrized as the sum of its individual diffuse power law spectrum and a common source term with an exponential cutoff parameter E_S:

$$\Phi_{e^+} = C_{e^+} E^{-\gamma_{e+}} + C_S E^{-\gamma_S} e^{-\frac{E}{E_S}} \tag{2}$$

$$\Phi_{e^-} = C_{e^-} E^{-\gamma_{e-}} + C_S E^{-\gamma_S} e^{-\frac{E}{E_S}}. \tag{3}$$

A fit of this model to the data of the positron fraction and to the ($e^+ + e^-$) flux allows the determination of all the parameters. The measurement and the resulting fit are shown in Figs. 2a and 2b. Figures 2c and 2d show the curve predicted from the fit together with

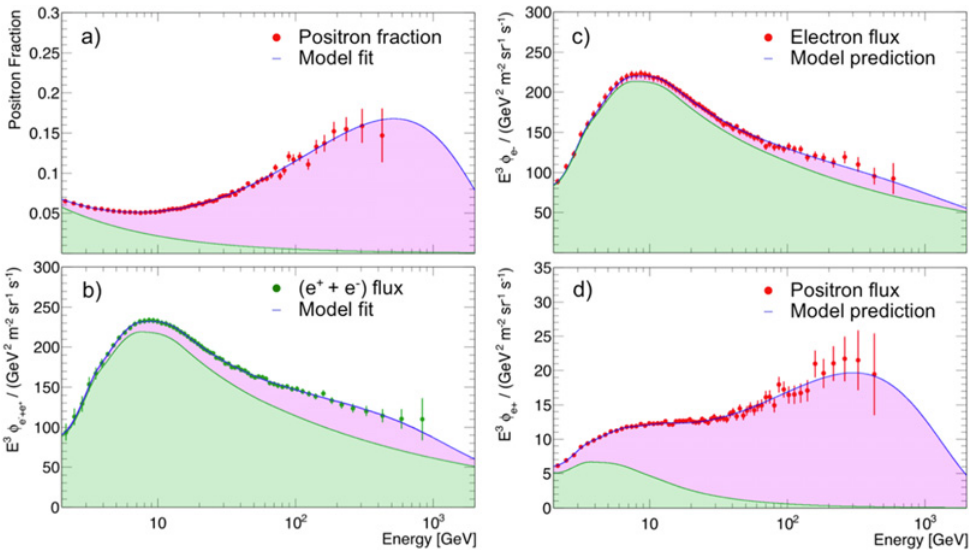

Figure 2. The positron fraction (panel a) and the total ($e^+ + e^-$) flux (panel b) are fitted with a simple model described in Sect. 6. Once the parameter are determined, the model prediction is drawn in panel c and d where the electron flux and positron flux are shown. In all panels the filled green area represents the diffuse flux component and the filled magenta area is the source component.

the measured electron and positron spectra. There is a nice agreement between the fit and the measured points showing that cosmic rays positrons and electrons are not consistent with only diffuse power law component: an additional source is needed to explain the measured positron fraction and the positron and electron fluxes.

This work is supported at the ASI Science Data Center under ASI-INFN agreements C/011/11/1 and No. 2014-037-R.0

References

[1] L. Feng et al., Phys. Lett. B **728** 250 (2014); K. Blum et al., Phys. Rev. Lett. **111**, 211101 (2013); L. Bergströ et al., Phys. Rev. Lett. **111**, 171101 (2013); I. Cholis et al., Phys. Rev. D **88**, 023013 (2013); T. Linden et al., Astrophys. J. **772**, 18 (2013)
[2] A. Kounine, Int. J. Mod. Phys. E **21**, 1230005 (2012); B. Bertucci, Proc. Sci., EPS-HEP (2011) 67; M. Incagli, AIP Conf. Proc. **1223**, 43 (2009); R. Battiston, Nucl. Instrum. Methods Phys. Res., Sect. A **588**, 227 (2008)
[3] M. Aguilar et al., Phys. Rev. Lett. **110**, 141102 (2013)
[4] B. P. Roe et al., Nucl. Instrum. Methods Phys. Res., Sect. A **543**, 577 (2005)
[5] C. Størmer, The Polar Aurora (Oxford University Press, London, 1950)
[6] L. Accardo et al., Phys. Rev. Lett. **113**, 121101 (2014)
[7] P. D. Serpico, Astropart. Phys. **39–40**, 2 (2012); T. Delahaye et al., Astron. Astrophys. **501**, 821 (2009); I. V. Moskalenko et al., Astrophys. J. **493**, 694 (1998)
[8] M. Aguilar et al., Phys. Rev. Lett. **113**, 121102 (2014)
[9] J. L. Bazo, this conference proceedings; M. Aguilar et al., Phys. Rev. Lett. **113**, 221102 (2014)